Chem Soc Rev

REVIEW ARTICLE

View Article Online
View Journal | View Issue



Cite this: *Chem. Soc. Rev.*, 2014, 43, 2662

# From charge transport parameters to charge mobility in organic semiconductors through multiscale simulation

Zhigang Shuai,*[a] Hua Geng,*[b] Wei Xu,[b] Yi Liao[c] and Jean-Marie André†[a]

This review introduces the development and application of a multiscale approach to assess the charge mobility for organic semiconductors, which combines quantum chemistry, Kinetic Monte Carlo (KMC), and molecular dynamics (MD) simulations. This approach is especially applicable in describing a large class of organic semiconductors with intermolecular electronic coupling ($V$) much less than intramolecular charge reorganization energy ($\lambda$), a situation where the band description fails obviously. The charge transport is modeled as successive charge hopping from one molecule to another. We highlight the quantum nuclear tunneling effect in the charge transfer, beyond the semiclassical Marcus theory. Such an effect is essential for interpreting the "paradoxical" experimental finding that optical measurement indicated "local charge" while electrical measurement indicated "bandlike". Coupled MD and KMC simulations demonstrated that the dynamic disorder caused by intermolecular vibration has negligible effect on the carrier mobility. We further apply the approach for molecular design of n-type materials and for rationalization of experimental results. The charge reorganization energy is analyzed through decomposition into internal coordinates relaxation, so that chemical structure contributions to the intramolecular electron–phonon interaction are revealed and give helpful indication to reduce the charge reorganization energy.

Received 4th September 2013

DOI: 10.1039/c3cs60319a

www.rsc.org/csr

## 1. Introduction

Organic materials play an important role in next-generation electronic applications, due to their processability and flexibility. However, low charge mobility and poor stability have restricted their development. Although some new molecular materials emerged with room-temperature mobilities up to tens $cm^2\ V^{-1}\ s^{-1}$,[1] a complete understanding of the charge transport mechanism is still not yet reached.[2–5] Electron–local phonon interaction model proposed by Holstein[6,7] depicted a general scheme for charge transport in organic solids. Non-local electron–phonon coupling had been included in Hostein–Peierls model by Munn–Silbey[8] and Hannewald–Bobbert.[9] Mixed quantum-classical (quantum for electrons and classical for atoms) non-adiabatic dynamics have been proposed with local electron–phonon coupling by Hultell and Stafstrom[10] and non-local electron–phonon coupling by Troisi and Orlandi.[11] However, mapping a complex molecular system onto a simple model even with both local and non-local couplings may lose important aspects of the structure features.[4] From the point of view of material design, a microscopic while realistic model for the intrinsic property is highly desirable. Some polyacenes single crystals indicate band-like charge transport.[12] According to the magnitude of electron–phonon interaction, different charge transport models have been adopted: (i) band model based on delocalized charge picture, where the intermolecular electron coupling ($V$) is much larger than the molecular reorganization energy ($\lambda$); (ii) intermediate regime, where $V$ is comparable to $\lambda$. None of these interactions can be treated as a perturbation, and all relevant interactions should be treated on the same footing.[13–18] (iii) $V$ is much less than $\lambda$, and the electron interacts strongly with intramolecular vibrations which eventually lead to self-localization: hopping model applies in this case. Although the localized charge model proposed by Brédas *et al.*[19] has achieved great successes in molecular design to achieve high charge mobility,[20–26] there are still some issues unsolved,[26] such as the involvement of molecular excited states of the ions in evaluating the electronic coupling term, the treatment of site variability, especially for amorphous organic films,[28] and the involvement of the nuclear tunneling effect in the charge transfer process.[29]

[a] *Key Laboratory of Organic OptoElectronics and Molecular Engineering, Department of Chemistry, Tsinghua University, 100084 Beijing, China. E-mail: zgshuai@tsinghua.edu.cn, hgeng@iccas.ac.cn*

[b] *Key Laboratory of Organic Solids, Beijing National Laboratory for Molecular Sciences (BNLMS), Institute of Chemistry, Chinese Academy of Sciences, 100190 Beijing, China*

[c] *Department of Chemistry, Capital Normal University, Beijing 100048, China*

† On leave from the Department of Chemistry, University of Namur, Belgium.

Marcus semi-classical theory[30] relied on classical treatment of nuclear motions in organic semiconductors.[19,31,32] The charge is localized in one molecule and the transport is carried out through the hoping process from one molecule to another *via* the charge transfer.[33,34] We recall that in studying the charge transfer process of the ferrous–ferric electron exchange reaction, Marcus originally assumed that electron transfer takes place after solvent reorganization, the charge solvation process being mainly associated with low frequency polarization motion ($\omega \ll kT$).[29] Therefore, the solvent polarization and fluctuation of the environment is described classically and vanishes with decreasing temperature. Hence, the semi-classical Marcus electron transfer theory predicts that the macroscopic current vanishes if the temperature approaches absolute zero. However, in organic semiconductors, the environment of the electrons consists of phonons, both intra-molecular and intermolecular, which often possess high frequency $\omega \gg kT$. Thus, the classical treatment for the environment is not appropriate for organic materials. In fact, a number of experiments have shown that the conductivity of organic materials at low temperatures is finite,[35–38] which demonstrates obvious quantum nuclear tunneling effects in organic semiconductors and the semi-classical approaches break down at low temperature. Quantum effect for charge transfer process have been considered by Jortner with a single effective high frequency vibration mode,[39] and by Emin[40,41] for polaron conductivity. Even for the original classical ferrous–ferric electron exchange reaction, quantum Monte-Carlo simulation treating water solvent quantum mechanically already demonstrated significant nuclear tunneling effects

**Zhigang Shuai**

*Zhigang Shuai, PhD 1989 Fudan University. 1990–2001, postdoc and research scientist the University of Mons, Belgium. 2002–2008, "Hundre-Talent" professor at the Institute of Chemistry of the Chinese Academy of Sciences in Beijing. 2008–date, Changjiang Scholar Chair professor, Tsinghua University, Beijing. His research interests are theoretical chemistry and modeling of the organic functional materials for opto-electronic properties. 278 publications with h-index 48. Outstanding Young Investigator's Fund (2004) and the Chinese Chemical Society–AkzoNobel Chemical Sciences Award (2012). Member of the International Academy of Quantum Molecular Science, the Royal Academy of Belgium, and Fellow of the Royal Society of Chemistry.*

**Hua Geng**

*Hua Geng graduated with a MSc degree in physics from Tianjin University. Since 2003, she became a research assistant with Professor Zhigang Shuai. She received her PhD degree supervised by Prof. Zhigang Shuai from the Institute of Chemistry of the Chinese Academy of Sciences in 2012. Currently, her research interests are theoretical evaluation of electron–phonon scatterings and charge transport in organic semiconductors.*

**Wei Xu**

*Wei Xu, received his PhD degree from the Chemistry Department, Wuhan University in 1997. After working as a Postdoc in Professor Daoben Zhu's group in the Institute of Chemistry of the Chinese Academy of Sciences, he obtained a permanent research scientist position there. Currently, he holds a research professor position. His research interests focus on design, synthesis, and device fabrication of organic semiconductors and thermoelectric materials.*

**Yi Liao**

*Yi Liao obtained her BSc degree and MSc degree in the Department of Chemistry, Northeast Normal University in 1994 and 2003, respectively. She received her PhD from Jilin University in 2006 on computational studies of organic electroluminescent materials under the supervision of Prof. Jikang Feng. After postdoctoral work at Nanjing University in 2009, she joined the Department of Chemistry in the Capital Normal University in Beijing as a full professor. Her major research interests focus on the design and synthesis of organic optoelectronic materials with the aid of computational chemistry.*

from solvent polarization fluctuations,[42] which later have been confirmed by Marcus himself.[43,44] For organic semiconductors, Nan *et al.*[29] have proposed the all-mode quantum charge transfer rate formalism in line with the non-radiative rate formalism[45] to investigate quantum nuclear tunneling effects, while several authors have also considered this effect by taking one effective quantum mode, keeping a classical treatment of the other modes.[46,47] All these efforts pointed out the importance of quantum effects. Especially, under such a local picture with nuclear tunneling, the dynamic disorder was found to have negligible effect on the mobility,[48] in sharp contrast to the previous investigations.[49] Preliminary ultrafast spectroscopy experiments indeed confirmed that the dynamic disorder does not play an appreciable role in charge transport at the nanosecond scale,[50] rendering consolidated support for such a picture.

Our previous review[51] summarized our progress in developing computational tools for the assessment of charge mobility starting from Marcus theory. Here we summarize our recent developments in three aspects, namely, quantum nuclear tunneling effect, dynamic disorder, and an internal coordinate projection scheme for charge reorganization energy as well as its application for molecular design. This article is organized in the following way: Section 2 describes the quantum nuclear effect and its application in organic semiconductors. Section 3 introduces electron–phonon coupling from intra and intermolecular vibrations evaluated from first principle quantum chemistry calculations. Section 4 presents the application in n-type semiconductors and gives some strategies towards high mobility charge transport materials. The summary and the outlook are presented in Section 5.

**Jean-Marie André**

*Jean-Marie André received his PhD in 1968 from the Catholic University of Louvain, Belgium. After a postdoctoral stay with Prof. E. Clementi at IBM San Jose, he joined the University of Namur in 1971 as associate professor and then he was promoted to be a full professor in 1974. His research interests are methodological development for the electronic structure of polymers and nonlinear optical properties. He received the International Academy of Quantum Molecular Science Annual Medal in 1984 for his contribution in understanding the properties of polymers. He was awarded the Francqui Prize on Exact Sciences in 1991, the highest distinction for scientists in Belgium. He is the honorary President of the Royal Academy of Belgium, and the honorary fellow of the Chinese Chemical Society. He received the Doctor Honoris Causa from the University of Warsaw, Poland.*

## 2. Quantum nuclear tunneling effect for electron transfer in organic semiconductors

As for charge transfer in organic semiconductors, the localized charge strongly interacts with the high frequency intramolecular vibration, thus demanding quantum treatments of the nuclear vibrations. Even at absolute-zero temperature, the system processes a quantum mechanical "zero-point energy", which will reduce the barrier between initial state to final state, quantum effect of nuclear vibration, also called nuclear tunneling effect, eventually will play an important role in the charge transfer processes. In this section, we introduce the derivation of the full quantum charge transfer rate based on a perturbational approach. In addition, we introduce our implementation of nonlocal electron phonon coupling by kinetic Monte-Carlo simulation under the localized charge picture.

### 2.1 Methodologies for quantum nuclear tunneling and dynamic disorder effects in the hopping model

Full-mode quantum charge transfer rate can be derived from Fermi golden rule. Within Condon approximation, the contributions of the electronic state and of the nuclear vibrational states can be written separately and the charge transfer rate is:

$$k = \frac{2\pi}{\hbar^2} V^2 \sum_{\nu,\nu'} P_{i\nu} |\langle \Theta_{f\nu'} | \Theta_{i\nu} \rangle|^2 \delta(\omega_{f\nu',i\nu}) \quad (1)$$

Here, $V = |\langle \psi_f | H' | \psi_i \rangle|$ is the electronic coupling between the final (initial) electronic states, $P_{i\nu}$ is the Boltzmann distribution function of $\nu$-th vibrational quanta in the initial state, $\Theta_{i\nu(f\nu')}$ is the wave function of the initial (final) nuclear vibration, and $\omega_{f\nu',i\nu}$ is the energy difference between the final and initial vibronic states.

$$\omega_{f\nu',i\nu} = \omega_{fi} + \sum_{\nu_j} \sum_{\nu_j'} \left[ \left( \nu_j' + \frac{1}{2} \right) \omega_j' - \left( \nu_j + \frac{1}{2} \right) \omega_j \right] \quad (2)$$

Under the harmonic approximation, the nuclear vibration wave function can be written as a product of independent harmonic oscillators, $\Theta_{i\nu} = \prod_j \chi_{i\nu_j}(Q_j)$, $\Theta_{f\nu'} = \prod_j \chi_{f\nu_j'}(Q_j')$, and the distribution function of initial state is $P_{i\nu} = \prod_j P_{i\nu_j}$. The wave function of a harmonic oscillator is

$$\chi_{\nu_j}(Q_j) = \left( \beta_j / \sqrt{\pi} 2^{\nu_j} \nu_j! \right)^{1/2} H_{\nu_j}(\beta_j Q_j) \exp(-\beta_j^2 Q_j^2 / 2) \quad (3)$$

Where $\beta_j$ and $H_{\nu_j}$ are the Hermite polynomials. The distribution function for the collection of quanta $\{V_j\}$ of the initial state is given by:

$$\begin{aligned} P_{i\nu} &= \left[ \sum_{\nu} \exp\left( \frac{-E_{i\nu}}{k_B T} \right) \right]^{-1} \exp\left( \frac{-E_{i\nu}}{k_B T} \right) \\ &= \prod_j^N 2 \sinh \frac{\hbar \omega_j}{2 k_B T} \exp\left( -\hbar \omega_j \left( \nu_j + \frac{1}{2} \right) \Big/ k_B T \right) \end{aligned} \quad (4)$$

 

Expressing the $\delta$ function as a Fourier integral of time, eqn (1) becomes

$$k = \frac{V^2}{\hbar^2}\int_{-\infty}^{\infty} \mathrm{d}t \mathrm{e}^{it\omega_{\mathrm{fi}}} \prod_j G_j(t) \tag{5}$$

$$G_j(t) = \sum_{\nu_j}\sum_{\nu_j'} P_{i\nu_j}\left|\left\langle \chi_{f\nu_j'}\middle|\chi_{i\nu_j}\right\rangle\right|^2 \times \exp\left(it\left\{\left(\nu_j' + \frac{1}{2}\right)\omega_j' - \left(\nu_j + \frac{1}{2}\right)\omega_j\right\}\right)$$

Under the displaced harmonic oscillator approximation, the phonon frequency and the modes of the initial (final) vibration state obey the following relationships: $\omega_j = \omega_j'$, $\Delta Q_j = Q_j' - Q_j$. Then the charge transfer rate can be expressed as:

$$k = \frac{V^2}{\hbar^2}\int_{-\infty}^{\infty} \mathrm{d}t \exp\left\{it\omega_{\mathrm{fi}} - \sum_j S_j\left[(2n_j+1) - n_j\mathrm{e}^{-it\omega_j} - (n_j+1)\mathrm{e}^{it\omega_j}\right]\right\} \tag{6}$$

Where, the intermolecular coupling $V$ between molecules m and n can be obtained with the site-energy overlap correction method:[52]

$$V_{\mathrm{mn}} = \frac{V_{\mathrm{mn}}^0 - \frac{1}{2}(e_{\mathrm{m}} + e_{\mathrm{n}})O_{\mathrm{mn}}}{1 - O_{\mathrm{mn}}^2} \tag{7}$$

Here, $e_{\mathrm{m}} = \langle\Phi_{\mathrm{m}}|H|\Phi_{\mathrm{m}}\rangle$, $V_{\mathrm{mn}}^0 = \langle\Phi_{\mathrm{m}}|H|\Phi_{\mathrm{n}}\rangle$, and $O_{\mathrm{mn}} = \langle\Phi_{\mathrm{m}}|O|\Phi_{\mathrm{n}}\rangle$, where $\Phi_{\mathrm{m(n)}}$ is the frontier molecular orbital of the isolated molecule *m(n)* in the dimer structure. Namely, for hole (electron) transport, HOMO (LUMO) should be plugged in. $H$ and $O$ are respectively the dimer Hamiltonian and the overlap matrices. $\bar{n}_j = 1/(\mathrm{e}^{\hbar\omega_j/k_{\mathrm{B}}T} - 1)$ is the occupation number for the $j$-th phonon mode with frequency $\omega_j$, the intra-molecular vibration modes and frequencies can be determined by quantum chemical calculation, $S_j$ is the Huang–Rhys factor measuring the coupling strength between the carrier on-site energy and the $j$-th intramolecular vibration mode, which can be obtained from a normal mode analysis approach with DUSHIN program.[53] In this way, quantum effect arising from local electron–phonon coupling (Holstein-type) naturally enters into the electron transfer process.

In the limit of strong coupling $S \gg 1$, the short time approximation can be applied ($\mathrm{e}^{i\omega t} \approx 1 + i\omega t + (i\omega t)^2/2$). In the case of $\hbar\omega_j/k_{\mathrm{B}}T \ll 1$, *i.e.* high temperature approximation, the occupation number of phonons turn to $\bar{n}_j \approx k_{\mathrm{B}}T/\hbar\omega_j$, so that eqn (6) goes back to Marcus formula with $\lambda = \sum_j \lambda_j = \sum_j S_j\hbar\omega_j$, where $\lambda_i$ is the charge reorganization energy through the dominating $i$-th intramolecular vibration mode, by its electronic coupling upon going from the neutral to the charged state and *vice versa*.

Non-local electron–phonon coupling (Peierls type) arising from intermolecular low-frequency vibration has been considered as the major scattering sources for the charge transport in organic semiconductors, or the dynamic disorder limited transport model.[11] It is thus intriguing to see how dynamic disorder influences the charge transport in the hopping model. Namely, in eqn (1), $V$ was assumed to be constant under the Condon approximation. In practice, $V$ is fluctuating with time. Since the period of thermal fluctuation of the transfer integral is much larger than the time of a single charge transfer, therefore, the intermolecular motion is treated classically, as usually made in the literature. We incorporated the non-local electron–phonon couplings in the hopping picture through a two-step approach, namely, the transfer integrals are kept constant during the charge transfer processes and they are updated after each hopping step.[54] Classical MD simulations were performed to obtain nuclear vibration trajectories at different temperatures. For each MD snapshot, electronic coupling can be obtained from quantum chemical calculation based on frontier orbitals of a dimer. Through the discrete Fourier transformation, the time-varying electronic coupling $V$ can be expressed as:

$$V_{\mathrm{mn}}(t) = \langle V_{\mathrm{mn}}\rangle + \sum_{k=0}^{N/2} \mathrm{Re}\, V_k \cdot \cos(\omega_k t + \varphi_0) + \sum_{k=0}^{N/2} \mathrm{Im}\, V_k \cdot \sin(\omega_k t + \varphi_0) \tag{8}$$

where $N$ is the total number of MD snapshots, Re $V$ and Im $V$ are the amplitudes; on this basis, the contributions of intermolecular vibration modes to the transfer integral fluctuation can be obtained. The phase factor $\varphi_0$ for each Fourier component is randomly set as $r\omega_k t$, where $r$ is a random number uniformly distributed in [0,1], $\omega_k$ is the Fourier frequency, and $t$ is the total simulation time.

Only one single hopping step is especially insufficient to describe charge transport in inhomogeneous systems, since the mobility is a bulk parameter and so is related to the long range molecular packing. Therefore, random walk schemes to simulate the charge diffusion using the kinetic Monte-Carlo (KMC) technique has been proposed. The flow chart of the simulation is shown in Fig. 1. First, charge transport parameters local electron phonon coupling $\lambda$, and intermolecular electronic coupling $V$ was evaluated from a quantum chemistry level, starting from the XRD crystal structure experimentally determined and choosing an arbitrary molecule within the bulk as the starting point for the carrier, the charge is only allowed to hop to its nearest neighbor molecules; based on charge transfer parameters, full quantum charge transfer rates are computed for all the possible neighbors, and the next position of the charge carrier is chosen randomly from the neighbors with a probability $P_\alpha = k_{\mathrm{mn}} \Big/ \sum_{\mathrm{n}'(\neq \mathrm{n})} k_{\mathrm{mn}'}$, the residence time of carrier at site m is $1 \Big/ \sum_{\mathrm{n}} k_{\mathrm{mn}}$; combined classical MD and quantum chemistry method, the time-varying electronic coupling $V$ can be obtained, the evolution of electronic coupling obeys eqn (8); The simulation will be stopped when the diffusion distance exceeds the intermolecular spacing by 2–3 orders of magnitude.

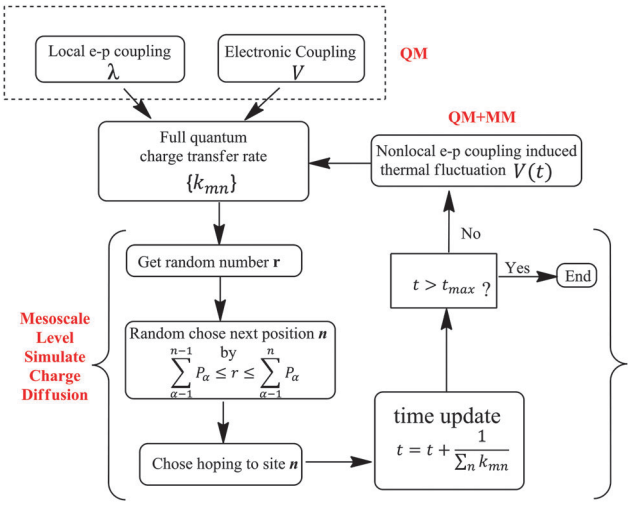


Fig. 1 Flow chart for multiscale charge diffusion simulation in organic semiconductors.

Thousands of KMC simulations must be performed to get a converged diffusion constant:

$$D = \frac{1}{2n} d\left\langle l(t)^2 \right\rangle \Big/ \mathrm{d}t, \qquad (9)$$

where $n$ is the spatial dimension, $l(t)$ is the distance of carrier's diffusion. Finally, charge mobility can be obtained through Einstein's relation $\mu = eD/k_BT$. Here, $e$ is the electron charge, and $k_B$ is the Boltzmann constant. It has been verified that both KMC and the Pauli master equation approach give essentially the same results and are found to be necessary for correct description for the mobility anisotropy.[27]

### 2.2 Tunneling enabled hopping model applied to pentacene derivatives

Polyacenes are typical organic semiconductors. However, these are not soluble nor air-stable materials. A variety of chemical modifications based on polyacenes has been carried out in order to achieve high mobility, solubility, and stability. 6,13-Bis(triisopropylsilyl ethynyl)-pentacene (**TIPS-P**) is a example of pentacene with good solubility and its charge transport properties have attracted extensive interest.[55] From electrical measurement, Sakanoue and Sirringhaus have recently reported a "bandlike" transport in **TIPS-P**. However, when they performed a charge modulation spectroscopy on the FET device, they observed a charge induced absorption peak at 1.3 eV, the same position as in the electrochemical doping in solution, indicating that the charge is localized on one single molecule in the FET device.[56] Compared with pentacene, **TIPS-P** reveals a much smaller intermolecular electronic coupling (about $V \sim 20$ meV for dimer A),[57] and a much larger intramolecular reorganization energy $\lambda$ (around 220 meV), namely, $V \ll \lambda$. Therefore, the localized charge picture is especially suitable to describe the charge transport properties in this case.

Based on their optimized molecular geometry for the neutral and singly charged molecules, the vibration frequencies and modes are calculated with the BhandHLYP DFT functional and with a 6-31G(d) basis set. The corresponding Huang–Rhys factors are obtained through normal mode analysis under the displaced harmonic oscillator approximation using the Dushin program. As can be seen in Fig. 2a, we found that the high frequency vibration plays a dominant role in the charge reorganization energy, indicating that quantum effect of intramolecular vibration should be considered.

Quantum charge transfer rates compared to the classical ones are given in Fig. 2(b). The classical Marcus CT rate increases with $T$, the characteristic of a thermal activation process. However, large charge transfer rates which originate from the quantum mechanical zero-point vibration energy have been found at low temperature. Therefore, the quantum rate is rather insensitive and slightly decreases when the temperature increases. However, the semi-classical Marcus rate only approaches the quantum rate around $T \sim 1000$ K, which means that the high temperature approximation is not applicable for organic semi-conductors at room temperature.

The dynamic disorder has been shown to play a dominant role within the small polaron model applied with the thermal average approximation.[55] Troisi *et al.* proposed a disorder-limited transport mechanism based on the Su–Schrieffer–Heeger model.[11] However, experimentally, no improvement in charge carrier mobility was observed at nanosecond time scales after pulsed

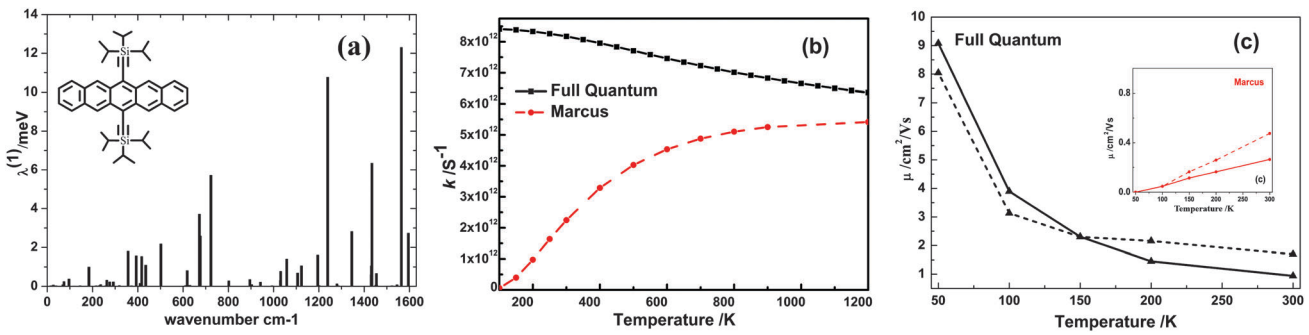


Fig. 2 (a) Contribution of the normal modes to the charge reorganization energy $\lambda^{(1)}$ from the singly positively charged molecule to the equilibrium structure of the neutral molecule. (b) Comparison of the hole transfer rates ($k$): black line for full quantum rate, and red line for semi-classical Marcus theory. (c) Hole mobility: dashed line for dynamic disorder and solid line for dynamically averaged static $V$'s. Classical Marcus rate result is shown in the inset. Adapted with permission from ref. 56. Copyright © 2012 Wiley-VCH Verlag GmbH & Co. KGaA, Weinheim.

 

photoexcitation when decreasing the dynamic disorder at low temperatures.[50] Therefore, the impact of the dynamic disorder on charge transport seems to support our approach (Fig. 2(c)). To generate many trajectories for a dimer, we adopt Molecular Dynamics (MD). Then, for each snapshot, we perform quantum chemical calculations, and the thermal fluctuation or dynamics disorder of the transfer integral can be obtained by the procedure outlined before and discussed in more detail in Section 3. In order to simulate the random diffusion of the carrier, a $30 \times 30 \times 1$ crystal lattice is constructed according to the parameters of unit cell. The probability of hopping from site m to the nearest neighbor site n is determined by $P_{mn} = \frac{k_n}{\sum_n k_{mn}}$. By averaging over 2000 trajectories, the diffusion constant is obtained. Finally, charge mobilities dependent on temperature are evaluated according to the Einstein formula. As depicted in Fig. 2(c), it should be noted that the tunneling enabled hopping model gives a $\frac{d\mu}{dT} < 0$ "bandlike" behavior for TIPS-pentacene, in sharp contrast to the classical Marcus theory (see inset figure). Therefore, we estimate that the band like charge transport is due to the quantum effect of the intramolecular high frequency vibration within the localized charge picture. In addition, the dynamic disorder has little effect on charge mobilities at lower temperature; however, it will enhance the mobility at room temperature.

# 3. Electron–phonon couplings with both intra- and inter-molecular vibrations

Organic molecules interact *via* weak van der Waals forces. As a consequence, the electronic states available for the charge carriers are spatially localized. Intermolecular electronic couplings ($V$) have been evaluated quantum chemically for many organic semiconductors.[58–60] Electron–phonon couplings are another important parameter in charge transfer processes, especially, in flexible organic semiconductors composed of light weighted atoms (C, S, N, H). The Hamiltonian including electron–phonon coupling is written as:

$$H_0 = H_0 + H_1 \tag{10}$$

$$H_0 = \sum_m \varepsilon_m a_m^+ a_m + \sum_{mn} t_{mn} a_m^+ a_n + \sum_l \hbar\omega_l \left( b_l^+ b_l + \frac{1}{2} \right) \tag{11}$$

$$H_1 = V_{\text{el-phonon}}^{\text{local}} + V_{\text{el-phonon}}^{\text{non-local}} \tag{12}$$

Here $a_m^+$ and $a_m$ denote the creation and annihilation operators for an electron at site (molecule) m; $t_{mn}$ represents the transfer integral between adjacent molecules as above mentioned; $\omega_l$ denotes the vibration frequency and $b_l^+$ and $b_l$ represent the creation and annihilation operators for a phonon at site l. Electron–phonon coupling is decomposed into: the local (Holstein-type) couplings and non-local (Peierls-type) couplings, according to the modulation of the site energies and electronic couplings:

$$V_{\text{el-phonon}}^{\text{local}} = \sum_l \sum_m \hbar\omega_l g_{l,mm} (b_l^+ + b_{-l}) a_m^+ a_m \tag{13}$$

$$V_{\text{el-phonon}}^{\text{local}} = \sum_l \sum_{m \neq n} \hbar\omega_l g_{l,mm} (b_l^+ + b_{-l}) a_m^+ a_m \tag{14}$$

Under the linear coupling approximation, the dimensionless $g_{l,mm}$ can be written as:

$$g_{l,mm} = (\hbar\omega_l^3)^{-1/2} \frac{\partial \varepsilon_m}{\partial Q_l} \tag{15}$$

In the case of non-polar molecules, the polarization of the surrounding molecules can be neglected in first approximation. The local electron–phonon coupling is dominated by the individual intra-molecular relaxation, or, in the context of Marcus electron-transfer theory, by the reorganization energy $\lambda$,

$$\lambda = \sum_l \hbar\omega_l g_{l,mm}^2 \tag{16}$$

In the same way, the dimensionless non-local electron phonon coupling constant $g_{l,mm}$ reads as:

$$g_{l,mm} = \left(\hbar\omega_l^3\right)^{-1/2} \frac{\partial \tau_{mm}}{\partial Q_l} \tag{17}$$

In the limit of low and high temperature,[61]

$$\sigma^2 = \sum_l \omega_l g_{l,mm}^2; \quad \hbar\omega \gg k_B T \tag{18}$$

$$\sigma^2 = 2k_B T \sum_l g_{l,mm}^2; \quad \hbar\omega \ll k_B T \tag{19}$$

Therefore, the strength of non-local electron–phonon coupling can be expressed from the thermal fluctuation of the transfer integral. In view of the low frequency character of the intermolecular vibration, the condition of $\hbar\omega \ll k_B T$ is fulfilled, and the dynamic disorder will follow a linear relationship with temperature.

### 3.1 Reorganization energy decomposition into internal coordinates

In order to clarify the contribution of the local structure relaxation to the reorganization energy, we have developed an internal-coordinate decomposition approach,[62] which identifies the segments that contribute the most to the reorganization energy. In conjunction with the frontier molecular orbital analysis, we can design functional groups at appropriate positions so as to reduce the charge reorganization energy.

**3.1.1 Methodology.** Charge reorganization energies are traditionally evaluated by the adiabatic potential energy surfaces (AP) method. The normal mode (NM) analysis is an alternative way under the harmonic oscillator approximation to obtain the vibronic relaxation contributions upon charge transfer, which, in many cases, are usually in good agreement with those obtained by the AP.[63,64] The NM analysis can also be used to simulate the UPS spectra. The agreement between the simulated and experimental spectra confirms the validity of DFT estimations

of reorganization energies.[63] Within the harmonic approximation, the total reorganization energy can be written as:

$$\lambda = \sum_{i} \lambda_i = \sum_{i} \frac{1}{2} \omega_i^2 \Delta Q_i^2 \quad (20)$$

Here, $\lambda_i$ is the reorganization energy from mode i with frequency $\omega_i$, $\Delta Q_i$ represents the displacement along the *i*-th normal mode coordinate between the equilibrium positions of the charged and neutral states. The total reorganization energy can be obtained by the summations over all vibrational modes. It is difficult to visualize the variation of the reorganization energy with respect to local structural modifications, since the normal modes are linear combination of all atomic displacements. In order to better understand the contribution of the local structure to the total reorganization energy, we proposed to decompose the total reorganization energy into internal coordinates, which allows the normal mode coordinates to be written as linear combinations of internal coordinates:

$$\Delta Q_i = \sum_{j} \alpha_{ij} \Delta S_j, \quad (21)$$

Substituting eqn (21) into eqn (20), the reorganization energy in terms of internal coordinates reads as:

$$\lambda = \sum_{j} \lambda(S_j) = \sum_{j} \sum_{i} \frac{\omega_i^2}{2} \left( \alpha_{ij}^2 \Delta S_j^2 + \sum_{m(\neq j)} \alpha_{ij} \alpha_{im} \Delta S_j \Delta S_m \right) \quad (22)$$

Here, $\lambda_j = \sum_i \frac{\omega_i^2}{2} \alpha_{ij}^2 \Delta S_j^2$ and $\lambda_{jm} = \sum_i \frac{\omega_i^2}{2} \sum_{m(\neq j)} \alpha_{ij} \alpha_{im} \Delta S_j \Delta S_m$ are the diagonal and non-diagonal terms respectively. When the non-diagonal terms in eqn (22) are small enough, the internal coordinate projection works appropriately. Assuming that there is no Duschinsky mixing and thus that the molecular charged state involved in electron transfer is characterized by the same force constants as the neutral state, the charge reorganization energy can be written as a function of the vibronic coupling constants:[3]

$$\lambda = \sum_{i} \lambda_i = \sum_{i} \frac{V_i^2}{2\omega_i^2} \quad (23)$$

The vibronic coupling constant $V_i$ for vibrational mode i becomes:

$$V_i = \left\langle \psi^+(\mathbf{r}, \mathbf{R}_0) \left| \left( \frac{\partial \mathbf{H}(\mathbf{r}, \mathbf{R})}{\partial Q_i} \right)_{\mathbf{R}_0} \right| \psi^+(\mathbf{r}, \mathbf{R}_0) \right\rangle \quad (24)$$

where, $\psi^+(\mathbf{r}, \mathbf{R}_0)$ is the wavefunction of the charged state at the optimized geometry ($R_0$) of the neutral state. By the conversion from normal coordinates to internal coordinates, the reorganization energy can be expressed as a function of the vibronic coupling constants in terms of internal coordinates:

$$\tilde{V}_i = \left\langle \psi^+(\mathbf{r}, \mathbf{R}_0) \left| \left( \frac{\partial \mathbf{H}(\mathbf{r}, \mathbf{R})}{\partial S_j} \right)_{\mathbf{R}_0} \right| \psi^+(\mathbf{r}, \mathbf{R}_0) \right\rangle \quad (25)$$

$$\lambda = \sum_{j} \lambda(\tilde{V}_j) = \sum_{j} \sum_{i} \frac{1}{2\omega_i^2} \left( \alpha_{ij}^2 \tilde{V}_j^2 + \sum_{m(\neq j)} \alpha_{ij} \alpha_{im} \tilde{V}_j \tilde{V}_m \right) \quad (26)$$

In contrast to expressions based on normal coordinates, eqn (26) provides a direct link between the reorganization energies and the local molecular properties. It contains also the non-diagonal contributions from the internal coordinates (and the related coupling constants). According to Koopmans' theorem, the hole vibronic coupling constant can be written in terms of normal coordinates:

$$V_i = \frac{\partial E_{HOMO}}{\partial Q_i} \quad (27)$$

In the tight-binding model, the energy of the HOMO can be expressed:

$$E_{HOMO} = C_1^2 \beta_{1,1} + C_1^2 \beta_{2,2} + 2C_1 C_2 \beta_{12} + 2C_1 C_3 \beta_{13} + \ldots \quad (28)$$

The variation of the vibronic coupling constants upon substitution can be related to modifications of the atomic charge densities:

$$\tilde{V}_i = \frac{\partial E_{HOMO}}{\partial S_i} = \sum_{j,k} C_j C_k \frac{\partial \beta_{j,k}}{\partial S_i} \quad (29)$$

$$\beta_{i,j} = \langle \phi_i | \mathbf{F} | \phi_j \rangle \quad (30)$$

Here, the $\phi_i$ terms form the atomic orbital basis in the LCAO tight-binding model, $\beta_{i,i}$, being the site energies, and $\beta_{i,j}$, the transfer integrals (resonance integral) between atoms i and j. In practice, the derivative of the resonance integral ($\beta_{i,j}$) between atoms i and j can be deduced from the dependence of the DFT Fock matrixelements on the inter-atomic bond lengths. In this way, we have established a link between the distribution of molecular orbital and the reorganization energy of corresponding segment.

**3.1.2 Case study of the substitution effect on indolo[3,2-*b*]-carbazole derivatives.** Substitution is an effective way both to improve molecular stacking[65] and to alter carrier type.[66] However, the reorganization energies have been found to increase significantly after chemical substitutions,[67,68] thus hindering charge transport. Here, we take typical hole transport materials like indolo[3,2-*b*]-carbazole derivatives as an example to analyze the chemical origin of the reorganization energy. The parent indolo[3,2-*b*]-carbazole molecule and its derivatives with two chlorine substituents at symmetrically equivalent positions are depicted in Fig. 3(a). The molecular geometries and the normal modes for the ground the charged states have been calculated using the B3LYP hybrid density functional in conjunction with the 6-31g(d) basis set as implemented in the Gaussian09 package.[69] The normal displacements $\Delta Q_i$ between the neutral state and the charged state are acquired through DUSHIN program.[53]

We found that the substitution position has a prominent effect on the reorganization energy, as shown in Fig. 3(b). The positions of the substituent largely influences the reorganization energy. Indeed, compared with the parent molecule (red line),

 

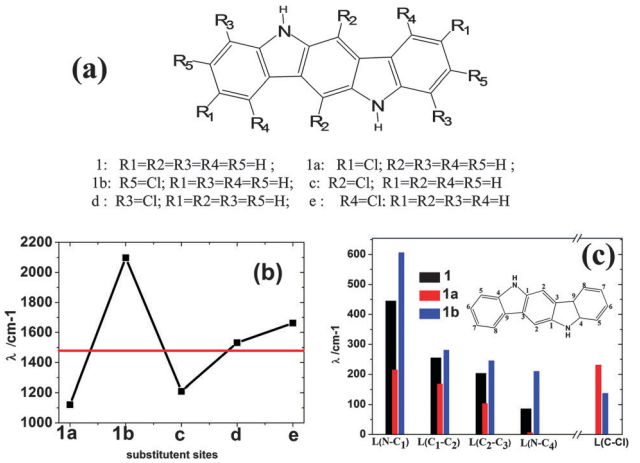


Fig. 3 (a) Molecular structures of **1**, **1a**, **1b**, **c**, **d**, and **e**. (b) Dependence of the calculated reorganization energy on substitution. The red line corresponds to the reorganization energy of unsubstituted indolo[3,2-*b*]carbazole. (c) Reorganization energy projected into internal bond-length coordinates for **1a**, **1b**, and **1**. Reprinted with permission from ref. 62. Copyright by AIP Publishing LLC.

the various substitutions can enhance reorganization energy or reduce it according to the position of the substituents. According to our internal coordinates' decomposition approach, the total reorganization energy can be related to the relaxation of bond lengths. We found that the relaxation processes along the C–Cl bonds significantly contribute to the reorganization energy, while the contributions from other coordinates are reduced (especially for N–$C_1$) for **1a**; thus, the overall reorganization energy turns out to be smaller than that observed for the parent molecule **1**. In contrast, the contributions from these bonds increase for **1b**, giving a much larger reorganization energy than the parent molecule **1** and **1a**. Namely, the pattern of chlorination significantly influences the relaxation along N–$C_1$ bonds.

Under Koopmans' approximation, the hole (electron) vibronic coupling along a specific bond is related to the product of the HOMO (LUMO) coefficients of the two atoms forming the bond, which is approximately equal to the bond order in the HOMO orbital if one neglects the atomic orbital overlap. The modification of the resonant integral derivatives upon chlorination is so small that it can be neglected. Therefore, the changes in relaxation energy along the N–$C_1$ bond originate from the modifications of the wavefunction amplitudes on the N and $C_1$ atoms upon substitution. As shown in Table 1, the smaller the charge density on the $C_1$ and N atoms, the smaller the reorganization energy of the bond N–$C_1$ will be. The large contribution of the bond length of N–$C_1$ can be understood from the polarization effect of nitrogen atoms.

Upon substitution, the charge distribution at some atoms of the conjugated system can be modified by long-range conjugation effects, or hyperconjugation. Indeed, if some proper substituent at a given position can influence the charge distribution at the nearby $C_1$ atoms so as to cancel the polarization effect of nitrogen atoms, the reorganization energy will be reduced, a result which is consistent with our molecular orbital analysis.

In summary, the reorganization energy decomposition approach makes it possible to establish a direct link between the local geometric structure and the reorganization energy. According to the modification of charge density distribution along a particular bond of the neutral state, we can predict the trends that will be observed in the modification of the charge reorganization energy. It allows us to choose appropriate substituents and proper positions to design organic semiconductors with low reorganization energy.

**3.1.3 Design of charge transport materials with small reorganization energy.** *N*-Heteropentacene (**N-PEN**) derivatives have attracted extensive interest as n-type semiconductors,[70–72] which can be classified into two kinds, the hydrogenated and dehydrogenated forms, corresponding to the "CH"/NH and "CH"/N substitutions on the PEN core, respectively. An interesting phenomenon concerning these **N-PEN** derivatives, noticed by us, is that the dehydrogenated forms always have better electron transport capability than the corresponding hydrogenated ones. Meanwhile, it has been found that the position of the N atoms plays an important role in tuning the structures and properties of organic semiconductors based on *N*-heteropentacenes.[73] Here we will analyze the role of the position of nitrogen atoms and of the dehydrogenation effect on the value of the reorganization energy.

To address the above issues, a series of *N*-heteropentacenes (**TIPS-N-PEN**s) derivatives, as depicted in Fig. 4, have been investigated at the single molecular level. We applied our reorganization energy decomposition approach to get a better insight into the effect of chemical modifications on the reorganization process associated with carrier transport. the equilibrium structures of neutral and ionic states were fully optimized for the above **N-PEN**s derivatives at the B3LYP/6-31G* level.

Based on adiabatic potential-energy surfaces, the reorganization energies due to the intramolecular vibrations have been evaluated. Upon going from hydrogenated **DHD(T)AP**s to the aromatic **D(T)AP**s, the hole and electron reorganization energies decrease from 35–106 meV and 66–265 meV, respectively. The prominent reduction in the reorganization energies for the

Table 1 HOMO molecular orbital coefficients on various atoms for compounds **1**, **1a**, and **1b**. Reprinted with permission from ref. 62. Copyright by AIP Publishing LLC

| | N | | $C_1$ | | $C_2$ | | $C_3$ | |
|---|---|---|---|---|---|---|---|---|
| Atomic orbital | 2PZ | 3PZ | 2PZ | 3PZ | 2PZ | 3PZ | 2PZ | 3PZ |
| **1** | 0.2759 | 0.2506 | −0.1546 | −0.1206 | −0.2028 | −0.1607 | 0.0846 | 0.0609 |
| **1a** | 0.2700 | 0.2452 | −0.1350 | −0.1062 | −0.2040 | −0.1616 | 0.0670 | 0.0483 |
| **1b** | 0.2758 | 0.2493 | −0.1619 | −0.1255 | −0.2060 | −0.1618 | 0.0861 | 0.0613 |

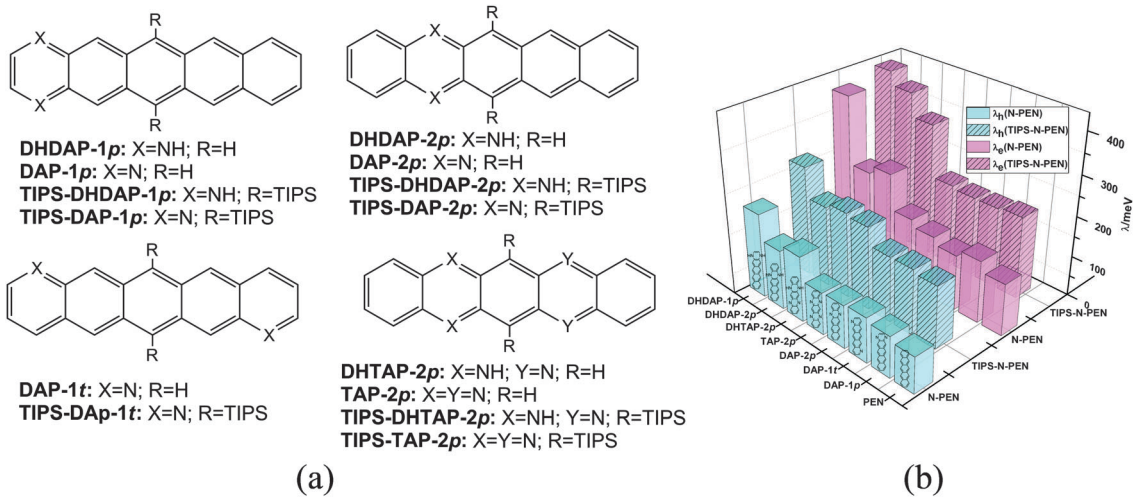


Fig. 4 (a) Molecular structures of the systems investigated, (b) the reorganization energies evaluated from the adiabatic potential-energy surface. Reprinted from ref. 60 with permission from The Royal Society of Chemistry.

aromatic **D(T)APs** can be partially ascribed to the larger delocalization degree of their frontier molecular orbitals compared to those of the formally anti-aromatic **DHD(T)APs**.

According to our reorganization energy decomposition approach, the local bonding characters of nitrogen atoms are closely connected with the reorganization energy. Therefore, the Natural Bond Orbital (NBO) method has been used to analyze the local bonding characters of the orbitals. As illustrated in Fig. 5, the contributions of the lone pair of N atoms to the HOMO and LUMO are 39% and 6% for the **DHDAP-1*p***, respectively. Upon dehydrogenation, **DAP-1*p*** displays an increased $sp^2$ character on the nitrogen atoms. The C–N bond of **DAP-1*p*** contains 5% bonding characters for the HOMO and 27% anti-bonding one for the LUMO. Therefore, extracting an electron or a hole will have more pronounced effects on the **DHDAP-1*p*** than on the **DAP-1*p***, since a larger contribution to the geometrical relaxation is expected from the delocalized $LP_N$ than from the bonding/anti-bonding C–N. However, a cyano substitution with non-bonding character of C–N has little effect on the reorganization energy.[74] Therefore, it can be understood that **DCP-2*p*** has the smallest $\lambda$ among all **N-PENs** studied here. We conclude that the contribution of the nitrogen part to the reorganization energy roughly follows the order: delocalized $LP_N$ > bonding or anti-bonding N > non-bonding N. The more intense is the delocalized $LP_N$, the more important the reorganization energy will be for the hydrogenated **DHDAP** systems; therefore, the reorganization energies of the **DHDAPs** could be readily modulated by judicious modification of the $LP_N$ components in the Froutier Molecular Orbitals. An effective strategy is to alter the position of nitrogen atoms from end rings (**DHDAP-1*p***) to center rings (**DHDAP-3*p***). As indicated in Fig. 5, the hole reorganization energies are reduced remarkably with the decreasing $LP_N$ components of the HOMOs from **DHDAP-1*p*** to **DHDAP-2*p*** and to **DHDAP-3*p***. However, considering that bonding and anti-bonding interactions dominate instead of $LP_N$ in the FMOs of **DAPs**, the reorganization energies of dehydrogenated **DAPs** are almost unaffected by the position of nitrogen atoms.

### 3.2 Intermolecular dynamic disorder effects through QM/MM study

There have been increasing interests on the non-local (Peierls-type) coupling in the charge-transport properties of many organic semiconductors.[3,75] Assuming that the vibration

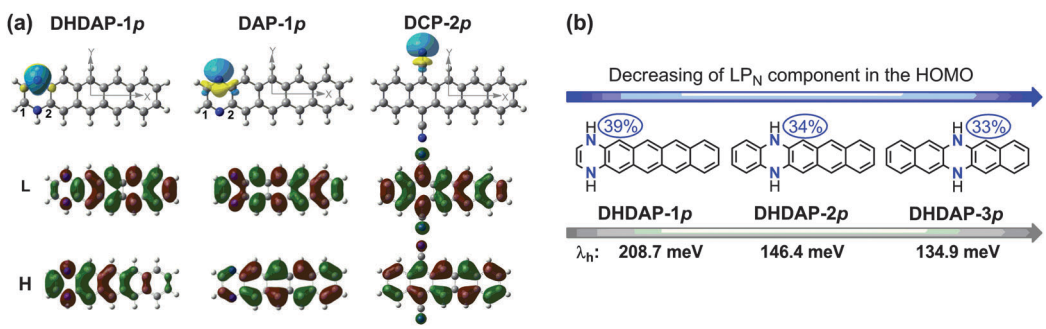


Fig. 5 (a) The frontier molecular orbitals and nitrogen NBO lone pair ($LP_N$) assignments of **DHDAP-1*p***, **DAP-1*p*** and **DCP-2*p***. (b) The $LP_N$ components in the HOMOs of **DHDAP-1*p***, **DHDAP-2*p*** and **DHDAP-3*p***. Reprinted from ref. 60 with permission from The Royal Society of Chemistry.

 

frequency does not change with temperature, the non-local electron–phonon coupling can be obtained through numerical derivation combined with a phonon modes calculation within the harmonic oscillator approximation.[76,77] Classical molecular-dynamics simulation is an alternative way to obtain time-dependent molecular geometries. Using these molecular geometries, the time evolution of the electronic coupling can be obtained from quantum chemical calculation. The strength of the non-local electron–phonon coupling can be evaluated by the thermal fluctuation of the transfer integral:

$$\sigma^2 = \langle (V_{mn} - \langle V_{mn} \rangle)^2 \rangle \quad (31)$$

In order to better understand the non-local electron–phonon coupling dependence on molecular structure, we have chosen pristine pentacene and its derivative tips-pentacene as examples. We have adopted a molecular dynamics (MD) approach to estimate the nuclear vibrations at different temperatures. A 5 × 5 × 3 and 3 × 3 × 3 super cell has been chosen for tips-pentacene and pristine pentacene respectively; therefore, the dimer that we are interested in is surrounded by many environmental molecules, so that artificial boundary effects can be prevented. The supercell structure can be seen in Fig. 6. The MD simulations have been run at constant temperatures every 50 K to 300 K using the Berendsen thermostat with the COMPASS force field. The system was first equilibrated for 60 ps in the NVT ensemble with a time step of 1 fs; after equilibration, a simulation of 120 ps has been run and 2000 frames were extracted by taking a snapshot every 60 fs along the trajectory.

Here, we choose the dimer A as an example. The intermolecular electronic couplings $V$ were calculated for each snapshot and the thermal fluctuation can be seen in Fig. 7(a). Through discrete Fourier transformation, the vibration frequency dependence on the amplitudes of periodic function is illustrated in Fig. 7(b). We found that TIPS-pentacene reveals a higher vibration frequency than that of pentacene. Both of them satisfy a Gaussian distribution, although the average transfer integral of pentacene is larger than that of tips-pentacene. The latter reveals a larger broadening than that of pentacene. The thermal fluctuation and dynamics

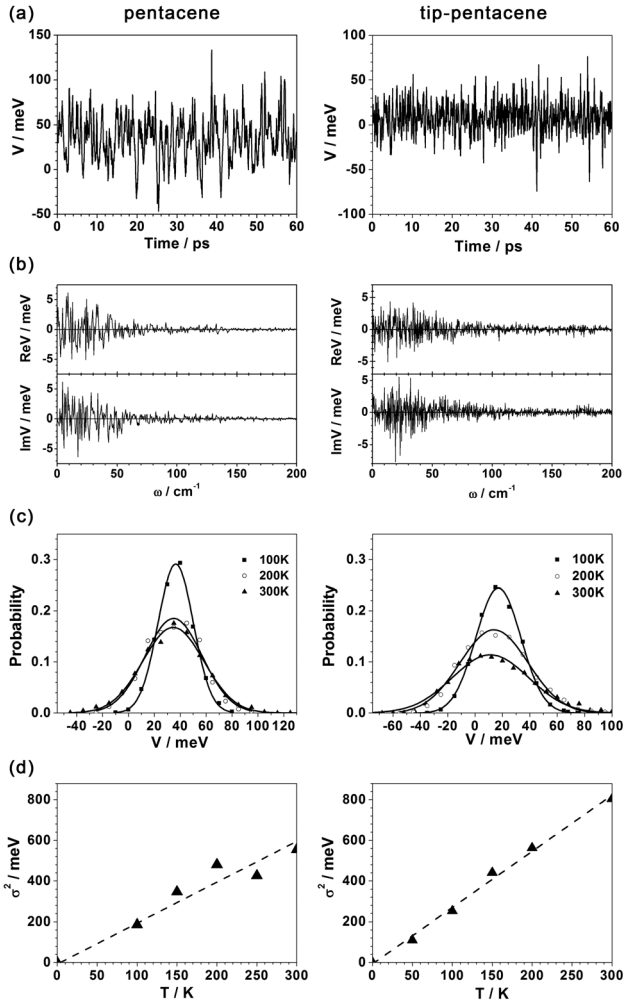


Fig. 7 (a) Thermal fluctuation of the transfer integral (dimer A) for pentacene (left) and tips-pentacene (right) at 300 K; (b) Fourier transformation of thermal deviation amplitude (ReV and ImV) at 300 K; (c) probability distribution of the transfer integral $V$ of dimer $A$. The solid line represents a Gaussian fit. (d) Square of the standard deviation of transfer integral as a function of temperature. (left) Reproduced from ref. 48 with permission from the Royal Society of Chemistry. (right) Reprinted with permission from ref. 56. Copyright © 2012 Wiley-VCH Verlag GmbH & Co. KGaA, Weinheim.

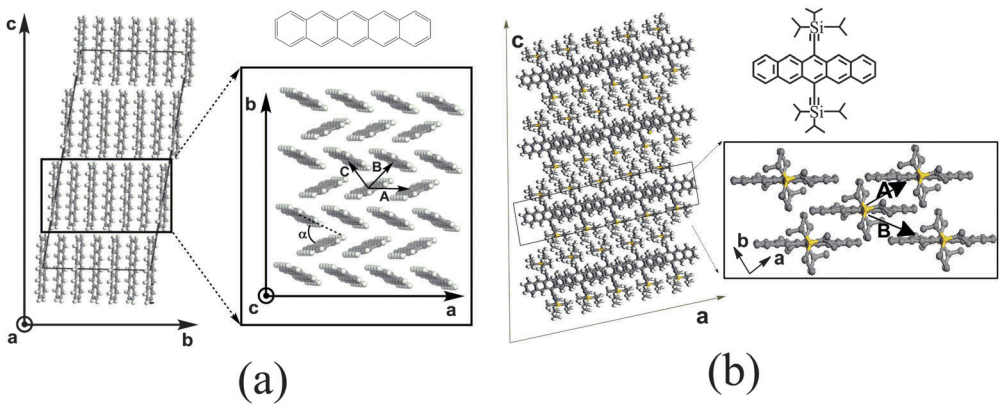


Fig. 6 (a) A 3 × 3 × 3 supercell structure of pentacene crystal, and an $a$–$b$ plane projection from the supercell. Reproduced from ref. 48 with permission from the Royal Society of Chemistry. (b) A 5 × 5 × 3 supercell structure of tips-pentacene crystal, and a $a$–$b$ plane projection from the supercell. Reprinted with permission from ref. 56. Copyright © 2012 Wiley-VCH Verlag GmbH & Co. KGaA, Weinheim.

disorder increase linearly with the temperature for both systems. When $\hbar\omega \ll k_BT$, the non-local electronic phonon coupling is the slope of the standard deviation, therefore, tips-pentacene displays a larger non-local electron–phonon coupling than that of pentacene. It maybe suggests that herringbone packing structures will have a smaller thermal fluctuation than that of brick π–π stacking structures, further investigation will be needed in this field.

# 4. Application to the molecular design of organic transport materials

Recently, tremendous progress has been achieved in molecular and polymeric semiconducting materials. Some p-type organic materials with a charge mobility comparable or even larger than amorphous silicon have been experimentally found.[78–81] However, the development of n-type semiconductors lags behind in both charge mobility and air stability. Quantum chemical calculations can provide useful information for molecular design in terms of the charge injection levels, air stability and molecular reorganization energy and intermolecular electronic couplings. Examples have been shown to be useful for the computational design of molecules of interest for high mobility organic semiconductors.[82] We have shown that a multi-scale approach starting from a molecule to charge diffusion in the entire bulk material can describe adequately the transport behaviors. Such an approach has been widely applied to the rationalization of experimental results on the novel n-type materials or on the donor–acceptor mixed co-crystal for achieving ambipolar materials. Some examples are discussed below.

## 4.1 Application to n-type organic semiconductors

To check the applicability of our theoretical simulation approach, we have applied it to a series of naphthalene, perylene diimide (NDI, PDI) derivatives and perfluoroalkyl modified oligothiophene where charge mobilities range from 0.1 to 6 $cm^2\ V^{-1}\ s^{-1}$.[79,83–88] The molecular structures are presented in Fig. 8. Experimentally measured charge mobility could depend on the device fabrication conditions, or on materials processing and impurities presented. Nevertheless, the theoretical results can be regarded as an intrinsic property of the materials, are helpful to rationalize the measurements and can serve as some standard to guide experiment.

The electron transfer integrals $V_e$ between the center molecule and all its neighbors are evaluated. The important electronic couplings from the main hopping pathways are illustrated in Fig. 8 for NDI derivatives. Among different substitutions, **1** exhibits a 2D brick stacking configuration, showing the largest transfer integral among the eight molecules (see left bottom of Fig. 8). **2** is a 1-D slipped-stacking structure possessing the second largest transfer integral. The other molecules have smaller electronic transfer integrals, less than 50 meV.

The geometric structure and the total energy of neutral and charge states have been calculated at the B3LYP/6-31G(d) level. The charge reorganization energies for electrons ($\lambda_e$) from normal mode analysis are in good agreement with the adiabatic potential approach for these systems, implying the adequacy of the harmonic oscilltor model. The magnitudes of $\lambda_e$ are all much larger than the intermolecular electron coupling $V$'s. According to a normal mode analysis, we found that the high frequency modes (1350–1700 $cm^{-1}$) play a dominant role in all the systems. For example, C=O and (single and double) C–C bond stretching

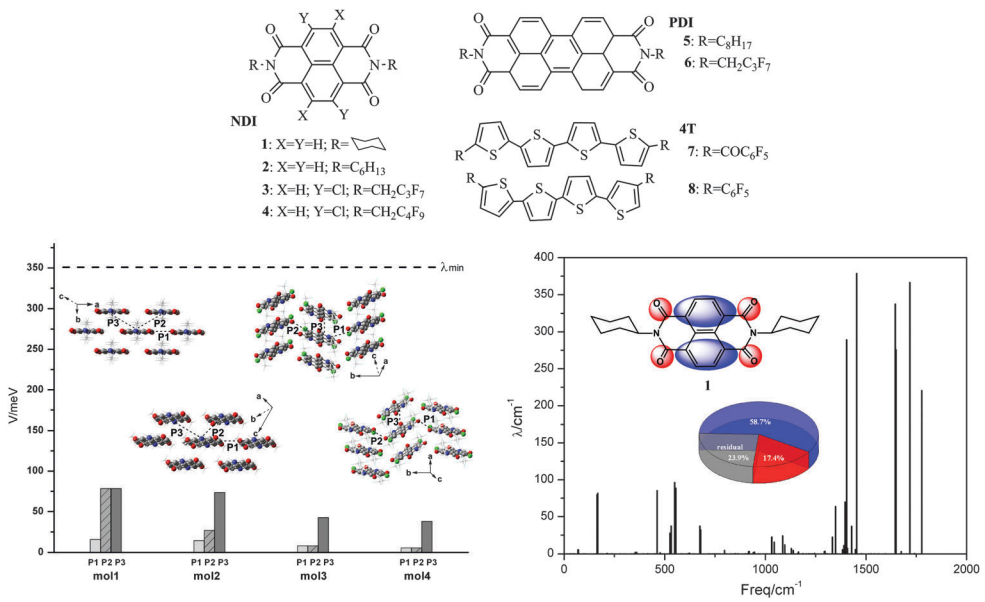


Fig. 8 (Top) molecular structures of the three types of n-type semiconductors, (left bottom) crystal packing for NDI derivatives with the electronic transfer integrals $V$ (meV) for main carrier hopping pathways P1–P3. The dashed line refers to the position of minimum reorganization energy. (Right bottom) contribution of the normal modes to the electron reorganization energy $\lambda_e$. The blue and red parts in the pie graph represent contributions from C–C single and double bond stretching modes and C=O stretching modes, respectively. Reprinted with permission from ref. 54. Copyright © 2012 Wiley-VCH Verlag GmbH & Co. KGaA, Weinheim.

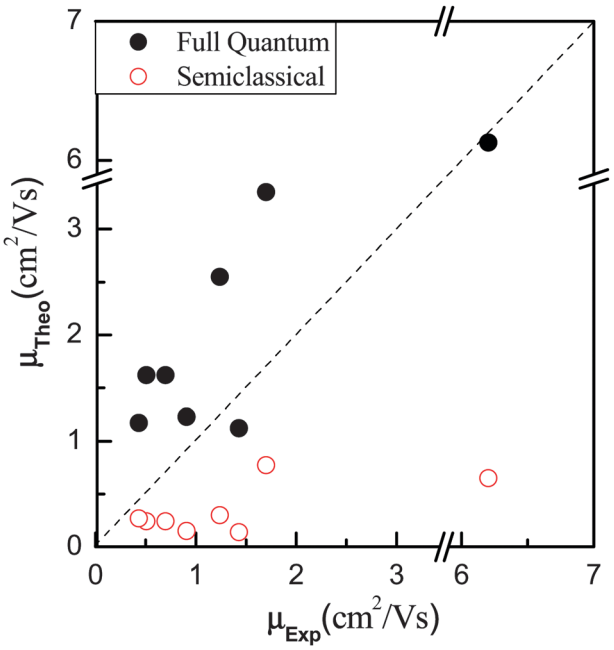


Fig. 9 Correlation between experimental and calculated electron mobility with full quantum and semiclassical Marcus methods. Reprinted with permission from ref. 56. Copyright © 2012 Wiley-VCH Verlag GmbH & Co. KGaA, Weinheim.

modes contribute to 17.4% and 58.7% for molecule **1**; other systems have similar contributions from high frequency vibration.

The semiclassical Marcus theory is not adequate when the localized charge is strongly coupled with the high frequency intramolecular vibration. Our tunneling-enabled hopping model is more suitable in these cases. Combined with kinetic Monte Carlo simulation, a full quantum charge transfer rate formula is adopted to evaluate the charge mobility of these systems, as shown in Fig. 9. It should be noted that our quantum charge transfer method correlates well with the experimental results. Marcus theory always underestimates charge mobility and even the trend does not correlate well with the experiment.

Fullerene ($C_{60}$), naphthalene diimides (NDI), and perylene tetracarboxylic diimides (PTCDIs) are typical n-type semiconductors. The electron mobility has reached as high as 6.0 $cm^2\ V^{-1}\ s^{-1}$ for the fullerene ($C_{60}$) manufactured OFET with a polymer as the dielectric layer. The electron mobility of cyclohexyl substituted NDI has reached 7.5 $cm^2\ V^{-1}\ s^{-1}$. Many derivatives of the PTCDI have been designed, synthesized and characterized with good conducting properties.[79,84] Some substitution groups have been introduced to improve the solubility and air stability, with the long alkane chain to prevent $H_2O$ and $O_2$ contamination to some extent. Cyano-substituted PTCDI derivatives have been found to have "band-like" character from 230 K to the room temperature[87] with the highest electron mobility up to 6.0 $cm^2\ V^{-1}\ s^{-1}$.[88] Therefore, taking PTCDI as an example (Fig. 10), we have investigated the relationship between charge mobility and the substitution groups, and from the temperature dependence, we discuss the charge transport mechanism.

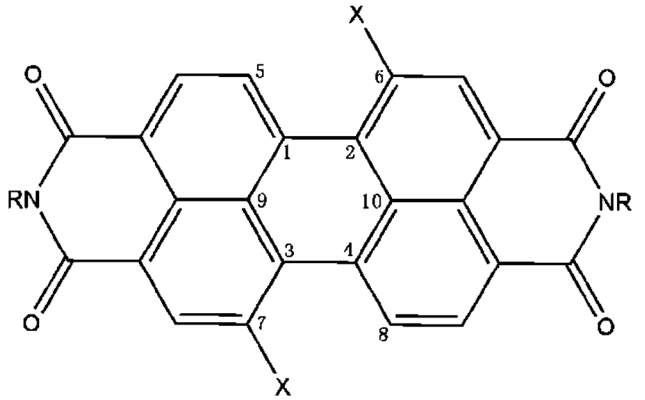


Fig. 10 Structure scheme of systems investigated. R = $CH_2C_3F_7$, X = H (**9**); X = CN (**10**); X = F (**11**); X = $C_4F_9$ (**12**).

Based on B3LYP functional and the 6-31G* basis set, the geometric structure of the neutral state has been optimized. Upon substitution at the bay positions of the PTCDI molecule, the conjugated core keeps almost its full planarity for systems **9**, **10** and **11**. However, the planarity of **12** is totally destroyed due to the steric hindrance of the substitution group, which is detrimental to the intermolecular stacking. Frontier molecular orbital profiles and energy levels are shown in Fig. 11, helpful for understanding the charge injection and air stability properties. The LUMO's of system **10** and **12** have been reduced remarkably, which suggests that high air stability could be achieved as n-type transport materials. The electron density of LUMO is mainly distributed at the perylene core for the four systems, while more delocalized electron distributions have been found in compounds **10** and **11**. Due to the non-bonding character of the cyano group, a lower reorganization energy is found, as expected from a model proposed by Chao *et al.*[89,90]

A normal mode analysis has been performed to investigate the dependence of reorganization energy on intramolecular vibration. The relaxation from neutral state to charged state and *vice versa* reveals similar trends for the contributions from the low frequency region (around 500 $cm^{-1}$) and the high frequency part (around 1500 $cm^{-1}$). The high frequency vibration mainly comes from the C=C in-plane stretching vibration. Similar distributions of the contributions to the reorganization energy of vibration modes have been found in the other three systems. Therefore, the quantum effect of nuclear vibration must be included in the charge transfer processes.

When decomposing the reorganization energy into the internal coordinates to reveal the substitution effect, as shown in Table 2, we observe that compound **12** has the largest reorganization energy, which is due to the $C_4F_9$ group causing additional contribution (about 18.2%), while the core part is almost not affected by the substitution. Compound **10** reveals less reorganization energy when compared with the other systems. The contribution of the core part is reduced upon cyano substitution, since the charge density distribution of the molecular orbital of the core part is well delocalized. Very little reorganization energy is introduced from the core substitution part (2.5%), which is consistent with the non-bonding character of the molecular orbital.

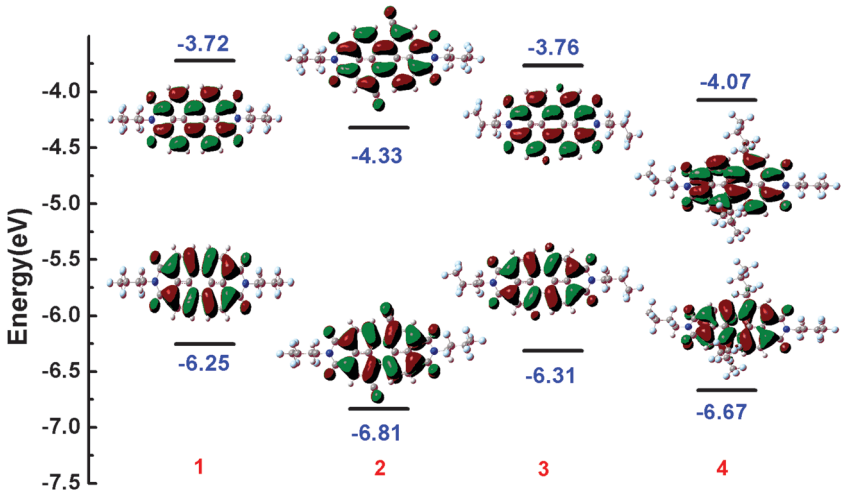


Fig. 11 Energy levels as well as charge density distribution of the HOMOs and LUMOs of compound **9–12**. Reprinted with permission from ref. 90. Copyright © 2012 Elsevier.

Table 2 Decomposition of the reorganization energy of four systems on the core (except the substitute groups), the end substitution groups and the core substitution groups. Reprinted with permission from ref. 91. Copyright © 2012 Elsevier

| | Compound | 9 | 10 | 11 | 12 |
|---|---|---|---|---|---|
| Core | *R*-energy ($cm^{-1}$) | 1066.07 | 998.67 | 1040.26 | 1034.71 |
| | Weight (%) | 91.0 | 90.5 | 86.1 | 69.4 |
| End substitutes | *R*-energy ($cm^{-1}$) | 104.94 | 76.93 | 118.71 | 184.40 |
| | Weight (%) | 9.0 | 7.0 | 9.8 | 12.4 |
| Core substitutes | *R*-energy ($cm^{-1}$) | <1.0 | 28.34 | 49.50 | 271.12 |
| | Weight (%) | — | 2.5 | 4.1 | 18.2 |

The intermolecular stacking configurations and corresponding electronic couplings as observed in Fig. 12 and Table 3. System **9** reveals one-dimensional π–π stacking configurations. However, system **10** displays a brick stacking configuration with closer intermolecular distances, and thus larger intermolecular electronic couplings. System **11** displays a herringbone packing character, and a large orbital overlap is found in the π–π stacking direction, while for the dimers with face to edge stacking, since the distance is large, the intermolecular electronic couplings have been found to be small. Due to the deformation of the core part of system **12**, the intermolecular distance is such that only the pathways P1 and P2 have noticeable electronic couplings. Therefore, system **10** possesses the best charge transport properties among the four compounds, with theoretical charge mobility as high as 16.96 $cm^2\ V^{-1}\ s^{-1}$, in comparison with the experimentally measured 6.0 $cm^2\ V^{-1}\ s^{-1}$.[87]

The temperature dependence for the four compounds is depicted in Fig. 13. As expected, the nuclear tunneling model always presents a decreasing behavior with temperature, as it would be in a "band-like" situation. Minder *et al.* have also found an experimental band like behaviour for compound **10**,[87] except for the thermally activated process below 210 K, since charge traps commonly existed in organic materials. When the carrier concentration is large enough to fill up all the defect levels, the nuclear tunneling effect can be found.[38]

Now we comment on the applicability of the Fermi golden rule here, since it is a first-order perturbation. Often, one is surprised by the success of the quantitative predictions by such a simple approximation. Recently, a more sophisticated electron wavepacket dynamics study has presented nearly identical results as

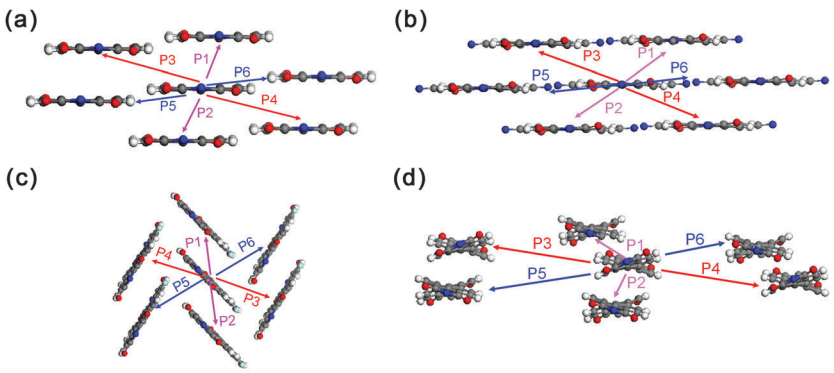


Fig. 12 Electron transfer pathways for system **9–12** corresponding to (a)–(d) respectively. along short-axis view. All the alkyl chain substitutions at the end of molecules are removed for clarity. Reprinted with permission from ref. 90. Copyright © 2012 Elsevier.

Table 3 Electronic coupling (meV) along different pathways for four systems. Reprinted with permission from ref. 90. Copyright © 2012 Elsevier

| Pathways | 9 | 10 | 11 | 12 |
|---|---|---|---|---|
| P1 | −0.23 | 67.94 | 110.29 | −84.32 |
| P2 | −0.23 | 67.94 | 110.28 | 27.75 |
| P3 | −39.44 | −84.74 | −1.58 | 0.00 |
| P4 | −39.44 | −84.74 | −1.58 | 0.00 |
| P5 | 5.55 | −4.57 | −1.58 | 0.00 |
| P6 | 5.55 | −4.57 | −1.58 | 0.00 |

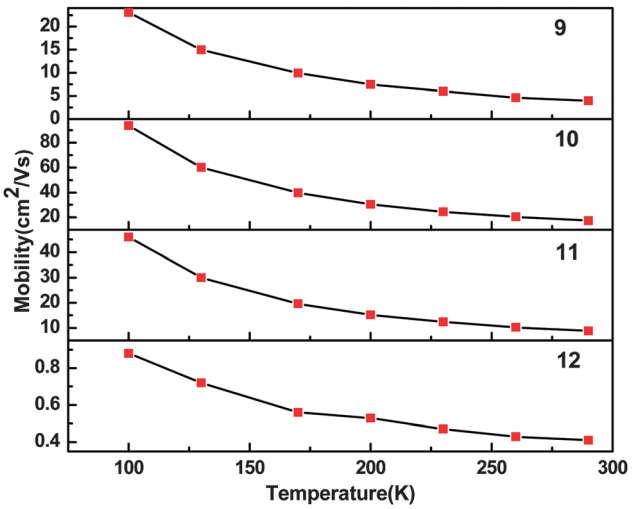


Fig. 13 Temperature dependence of electron mobility for the four PTCDI compounds. Reprinted with permission from ref. 90. Copyright © 2012 Elsevier.

the one obtained by the Fermi golden rule.[91,92] This is very encouraging to extend the application scopes of the present procedure.

### 4.2 Ambipolar charge transport in fullerene–sulfur-bridged annulene cocrystals

Ambipolar transport materials have attracted extensive interest, since (i) the fabrication of complementary-like circuits could be significantly simplified and (ii) the integration of light-emitting and field-effect transistors can be enabled, even achieving an electrically pumped lasing application. Recently, it has been found that the organic donor–acceptor (D–A) dyads constitute an efficient way to realize ambipolar operations. Wakahara *et al.*[93] reported an ambipolar transistor based on $C_{60}$–cobalt porphyrin (1 : 1) co-crystal with a balance electron and hole mobilities in the range of $10^{-5}$–$10^{-6}$ $cm^2\ V^{-1}\ s^{-1}$. Park *et al.*[94] have designed a donor–acceptor cocrystal with ambipolar field effect mobility up to $10^{-3}$ $cm^2\ V^{-1}\ s^{-1}$.

We have successfully synthesized a fullerene–sulfur-bridged annulene (DPTTA) cocrystal,[95] where both $C_{60}$ and $C_{70}$ have been employed as electron acceptors. The electronic structure is presented in Fig. 14. Large misalignments between frontier molecular orbital energy levels of donor and acceptor molecules exclude any super-exchange interaction between donors or between acceptors. $C_{60}$ and $C_{70}$ present similar adiabatic electron affinities (2.07, 2.15 eV respectively).

Since the cocrystal presents a two-dimensional segregated alternating layer structure, the electron transport mainly takes place in acceptor molecular layers, while holes are in the donor molecular (DPTTA) layers. Electron reorganization energies for $C_{60}$ and $C_{70}$ molecules are calculated to be 135 and 142 meV, respectively. While the hole reorganization energy calculated for the DPTTA donor molecule is 201 meV.

Electron and hole transport pathways in $C_{60}$–DPTTA are shown in Fig. 15. $C_{70}$–DPTTA presents a similar transport network except with different intermolecular distance and electronic coupling. The corresponding electronic coupling is listed in Table 4. Under Koopmans' approximation, transfer integrals for electron and hole are calculated from LUMO and HOMO, respectively. In the case of $C_{60}$ ($C_{70}$) molecules, LUMOs have three-fold (two-fold) degeneracy. The electronic couplings between any two degenerate molecular orbitals have been calculated. Supposing that the carriers initially satisfy the Boltzmann distribution, and can hop to any one degenerate energy level, the effective transfer integral can be derived as $V_{eff}^2 = \sum_{ij} P_i V_{ij}^2$, where $P_i$ is the Boltzmann distribution function for the initial state.

$C_{60}$–DPTTA shows isotropic electronic couplings for electron and hole. Obvious anisotropic electronic couplings can be found

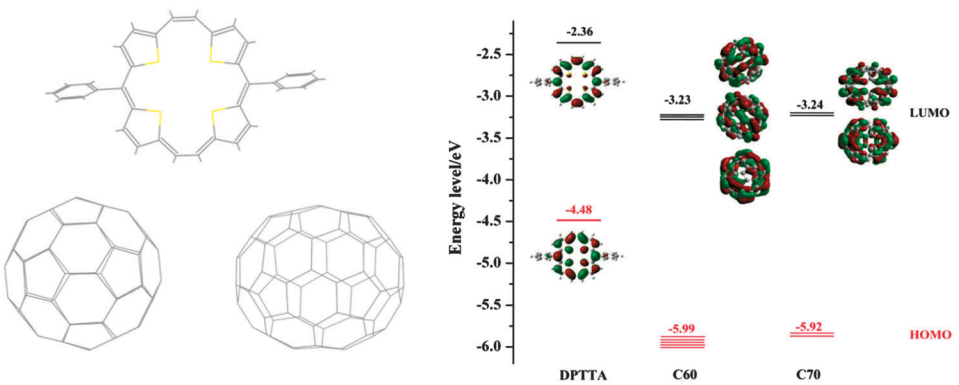


Fig. 14 Geometric and electronic structure of $C_{60}$, DPTTA, and $C_{70}$. Reprinted with permission from ref. 95. Copyright © 2013 American Chemical Society.

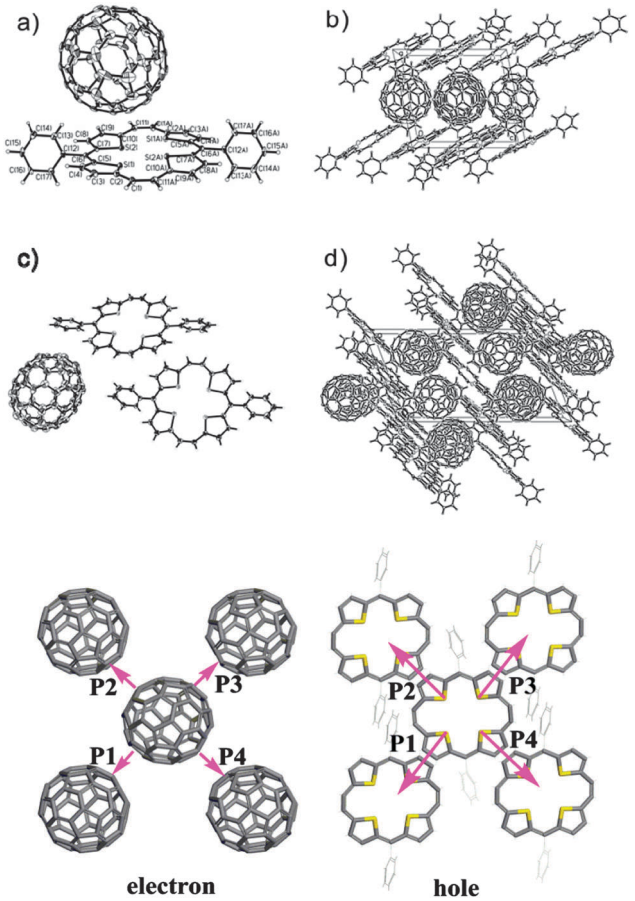


Fig. 15 Crystal structures of $C_{60}$–DPTTA and $C_{70}$–DPTTA. ORTEP drawings of the asymmetric unit of $C_{60}$–DPTTA (a) and $C_{70}$–DPTTA (c) showing thermal ellipsoids set at 50% probability level; stacking pattern in $C_{60}$–DPTTA (b) and $C_{70}$–DPTTA (d) view along the *b*-axis. Lower penal for illustration of charge hopping pathways schemes in the $C_{60}$ layer and DPTTA layer in co-crystal $C_{60}$–DPTTA. Reprinted with permission from ref. 95. Copyright © 2013 American Chemical Society.

for electrons in co-crystal $C_{70}$–DPTTA. Similar transfer integrals for the hole are found in both $C_{60}$–DPTTA and $C_{70}$–DPTTA cocrystals. Based on the above charge transfer parameters, our tunneling enabled hopping model coupled with kinetic Monte Carlo simulation has been performed to obtain two-dimensional average diffusion mobilities, given in Table 5. It is seen that intrinsically, the electron mobility is much larger than the hole mobility. However, the experimental results show lower electron mobilities especially in the $C_{60}$–DPTTA crystal.[95] This might be due to the fact that there are more traps for electrons than for holes in organic semiconductors and the semiconductor/dielectric interface.

Table 5 Charge mobility for electrons and holes in $C_{60}$–DPTTA and $C_{70}$–DPTTA systems

| Systems | Experiment $\mu_e$ ($cm^2\ V^{-1}\ s^{-1}$) | Theory $\mu_e$ ($cm^2\ V^{-1}\ s^{-1}$) | Experiment $\mu_h$ ($cm^2\ V^{-1}\ s^{-1}$) | Theory $\mu_h$ ($cm^2\ V^{-1}\ s^{-1}$) |
|---|---|---|---|---|
| $C_{60}$–DPTTA | 0.01 | 24 | 0.3 | 0.52 |
| $C_{70}$–DPTTA | 0.05 | 17 | 0.07 | 0.48 |

## 5. Conclusions and outlook

To summarize, we have presented a multiscale computational approach combining quantum charge transfer theory, molecular dynamics, and kinetic Monte Carlo simulations to assess the charge mobility in organic semiconductors. This model features intramolecular high frequency vibration relaxation upon molecular charging. Intermolecular vibration relaxation or dynamic disorder is modeled by Molecular Dynamics followed by quantum chemistry calculations for intermolecular coupling at each snapshot as well as kinetic Monte Carlo simulation. We found that (i) mobility decreases with increasing temperature resulting from a nuclear tunneling effect instead of the claimed "bandlike", which can also explain the contradictory optical measurements in TIPS-pentacene. Such an approach can also quantitatively predict charge mobilities for a series of n-type materials, including naphthalene and perylene diimide derivatives and perfluoroalkyl modified oligothiophenes.

Chemical substitution is often used to improve the performance and the stability of materials. But doing this often increases the reorganization energy thus lowering the mobility. We have presented a computational scheme to decompose the reorganization energy into molecular internal coordinates relaxations. Both substitution types and positions have strong influences on the reorganization energy. Our approach presents a quantitative analysis on the role of substitution, helpful for molecular design.

It should be noted that from both mechanism and computational chemistry points of views, there are still important challenges in modeling the charge transport phenomena towards quantitative description and prediction.[96] Organic materials cover both hopping and bandlike behaviors and the criterion is still arguable.[97] The role of both static and dynamic disorders in both charge and exciton transport has been regarded as essential and continuously explorable.[98] The work presented here is limited

Table 4 Transfer integrals and distances between center of mass of two molecules along different transfer pathways in the same layer in crystal $C_{60}$–DPTTA and $C_{70}$–DPTTA, respectively. Reprinted with permission from ref. 95. Copyright © 2013 American Chemical Society

| | Distance (Angstrom) | | $V^{eff}$/electron (meV) | | $V^{eff}$/hole (meV) | |
|---|---|---|---|---|---|---|
| | DPTTA–$C_{60}$ | DPTTA–$C_{70}$ | DPTTA–$C_{60}$ | DPTTA–$C_{70}$ | DPTTA–$C_{60}$ | DPTTA–$C_{70}$ |
| P1 | 10.02 | 10.59 | 34.75 | 34.15 | 12.31 | −1.28 |
| P2 | 10.02 | 10.59 | 34.75 | 34.17 | 12.31 | 14.59 |
| P3 | 10.02 | 10.59 | 34.75 | 27.93 | 12.31 | −1.28 |
| P4 | 10.02 | 10.59 | 34.75 | 27.94 | 12.31 | 14.60 |

to the dynamic disorder under the umbrella of tunneling enabled hopping model, which needs further extension to include static disorder as well as charge delocalization effects. For the bandlike description, even though knowledge from traditional inorganic semiconductor theory can be directly employed, the challenges arise from the description of electron–phonon scattering/relaxation with dispersion effect.[99] The computational methodology developments should go beyond the frontier orbital approximation. For example, the valence bond theory provided a natural way to construct the charge block state for the charge transfer processes in a complex environment.[100] Electron dynamics seems adequate to be applied to charge and exciton motion in organic systems as shown by Tretiak *et al*.[101] Further development to include quantum nuclear effect is desirable, since as shown in this review, the quantum nuclear tunneling is important in both organic semiconductors and conducting polymers. In one word, we are still a long way away from a full understanding of the transport behavior in organic materials.

## Acknowledgements

This work is supported by National Natural Science Foundation of China (Grant Nos. 21290191, 21303213, 91333202) and the Ministry of Science and Technology of China through 973 program (Grant Nos. 2011CB932304, 2011CB808405, and 2013CB933503). The following collaborators have made important contributions to the original work: Dr Linjun Wang, Dr Guangjun Nan, Dr Liping Chen, Dr Lili Lin, Prof. Yi Zhao, and Prof. Qiang Shi. JMA's scientific stay in Tsinghua is supported by the "Oversea Top Academic Visitor" (OTAV) Program of the Ministry of Education of China. H. Geng wishes to thank Prof. Yuanping Yi for valuable discussions. The numerical calculations have been done in the CNIC supercomputer center of the Chinese Academy of Sciences and the Tsinghua University Supercomputer Center.

## References

1 H. Minemawari, T. Yamada, H. Matsui, J. Y. Tsutsumi, S. Haas, R. Chiba, R. Kumai and T. Hasegawa, *Nature*, 2011, **475**, 364.
2 A. Troisi, *Org. Electron.*, 2010, **223**, 259–300.
3 V. Coropceanu, J. Cornil, D. A. da Silva Filho, Y. Olivier, R. Silbey and J.-L. Brédas, *Chem. Rev.*, 2007, **107**, 926–952.
4 Z. Shuai, L. Wang and Q. Li, *Adv. Mater.*, 2011, **23**, 1145–1153.
5 H. Bässler and A. Kohler, *Top. Curr. Chem.*, 2012, **312**, 1–65.
6 T. Holstein, *Ann. Phys.*, 1959, **8**, 325–342.
7 T. Holstein, *Ann. Phys.*, 1959, **8**, 343–389.
8 R. W. Munn and R. Silbey, *J. Chem. Phys.*, 1985, **83**, 1843–1853.
9 K. Hannewald and P. A. Bobbert, *Appl. Phys. Lett.*, 2004, **85**, 1535.
10 M. Hultell and S. Stafstrom, *Chem. Phys. Lett.*, 2006, **428**, 446.
11 A. Troisi and G. Orlandi, *Phys. Rev. Lett.*, 2006, **96**, 086601.
12 S.-i. Machida, Y. Nakayama, S. Duhm, Q. Xin, A. Funakoshi, N. Ogawa, S. Kera, N. Ueno and H. Ishii, *Phys. Rev. Lett.*, 2010, **104**, 156401.
13 Y. Li, Y. Yi, V. Coropceanu and J.-L. Brédas, *Phys. Rev. B: Condens. Matter Mater. Phys.*, 2012, **85**, 245201.
14 L. Wang and D. Beljonne, *J. Phys. Chem. Lett.*, 2013, **4**, 1888–1894.
15 S. Ciuchi and S. Fratini, *Phys. Rev. Lett.*, 2011, **106**, 166403.
16 F. Gargiulo, C. A. Perroni, V. M. Ramaglia and V. Cataudella, *Phys. Rev. B: Condens. Matter Mater. Phys.*, 2011, **84**, 245204.
17 V. Cataudella, G. De Filippis and C. A. Perroni, *Phys. Rev. B: Condens. Matter Mater. Phys.*, 2011, **83**, 165203.
18 J. F. Ren, N. Vukmirovic and L. W. Wang, *Phys. Rev. B: Condens. Matter Mater. Phys.*, 2013, **87**, 205117.
19 J. L. Brédas, J. P. Calbert, D. A. da Silva Filho and J. Cornil, *Proc. Natl. Acad. Sci. U. S. A.*, 2002, **99**, 5804–5809.
20 A. N. Sokolov, S. Atahan-Evrenk, R. Mondal, H. B. Akkerman, R. S. Sanchéz-Carrera, S. Granados-Focil, J. Schrier, S. C. B. Mannsfeld, A. P. Zoombelt, Z. Bao and A. Aspuru-Guzik, *Nat. Commun.*, 2011, **2**, 437.
21 L. Q. Li, Q. X. Tang, H. X. Li, X. D. Yang, W. P. Hu, Y. B. Song, Z. G. Shuai, W. Xu, Y. Q. Liu and D. B. Zhu, *Adv. Mater.*, 2007, **19**, 2613.
22 X. D. Yang, L. J. Wang, C. L. Wang, W. Long and Z. G. Shuai, *Chem. Mater.*, 2008, **20**, 3205–3211.
23 X. D. Yang, Q. K. Li and Z. G. Shuai, *Nanotechnology*, 2007, **18**, 24029.
24 B. Zhang, Y.-H. Kan, Y. Geng, Y.-A. Duan, H.-B. Li, J. Hua and Z.-M. Su, *Org. Electron.*, 2013, **14**, 1359–1369.
25 H. Li, L. Duan, Y. Sun, D. Zhang, L. Wang and Y. Qiu, *J. Phys. Chem. C*, 2013, **117**, 16336–16342.
26 X.-K. Chen, L.-Y. Zou, S. Huang, C.-G. Min, A.-M. Ren, J.-K. Feng and C.-C. Sun, *Org. Electron.*, 2011, **12**, 1198–1210.
27 S. Yin, L. Li, Y. Yang and J. R. Reimers, *J. Phys. Chem. C*, 2012, **116**, 14826–14836.
28 V. Ruehle, A. Lukyanov, F. May, M. Schrader, T. Vehoff, J. Kirkpatrick, B. Baumeier and D. Andrienko, *J. Chem. Theory Comput.*, 2011, **7**, 3335–3345.
29 G. J. Nan, X. D. Yang, L. J. Wang, Z. G. Shuai and Y. Zhao, *Phys. Rev. B: Condens. Matter Mater. Phys.*, 2009, **79**, 115203.
30 R. A. Marcus, *J. Chem. Phys.*, 1956, **24**, 966–978.
31 J. Cornil, D. Beljonne, J. P. Calbert and J. L. Brédas, *Adv. Mater.*, 2001, **13**, 1053.
32 D. A. da Silva, E. G. Kim and J. L. Brédas, *Adv. Mater.*, 2005, **17**, 1072.
33 W. Q. Deng and W. A. Goddard III, *J. Phys. Chem. B*, 2004, **108**, 8614.
34 Y. B. Song, C. A. Di, X. D. Yang, S. P. Li, W. Xu, Y. Q. Liu, L. M. Yang, Z. G. Shuai, D. Q. Zhang and D. B. Zhu, *J. Am. Chem. Soc.*, 2006, **128**, 15940–15941.
35 J. D. Yuen, R. Menon, N. E. Coates, E. B. Namdas, S. Cho, S. T. Hannahs, D. Moses and A. J. Heeger, *Nat. Mater.*, 2009, **8**, 572–575.
36 A. J. Kronemeijer, E. H. Huisman, I. Katsouras, P. A. van Hal, T. C. T. Geuns, P. W. M. Blom, S. J. van der Molen and D. M. de Leeuw, *Phys. Rev. Lett.*, 2010, **105**, 156604.

37 A. S. Dhoot, G. M. Wang, D. Moses and A. J. Heeger, *Phys. Rev. Lett.*, 2006, **96**, 246403.
38 K. Asadi, A. J. Kronemeijer, T. Cramer, L. J. A. Koster, P. W. M. Blom and D. M. de Leeuw, *Nat. Commun.*, 2013, **4**, 1710.
39 N. R. Kestner, J. Logan and J. Jortner, *J. Phys. Chem.*, 1974, **78**, 2148–2166.
40 D. Emin, *Adv. Phys.*, 1975, **24**, 305–348.
41 E. Gorhambergeron and D. Emin, *Phys. Rev. B: Condens. Matter Mater. Phys.*, 1977, **15**, 3667–3680.
42 J. S. Bader, R. A. Kuharski and D. Chandler, *J. Chem. Phys.*, 1990, **93**, 230–236.
43 X. Y. Song and R. A. Marcus, *J. Chem. Phys.*, 1993, **99**, 7768–7773.
44 Y. Georgievskii, C. P. Hsu and R. A. Marcus, *J. Chem. Phys.*, 1999, **110**, 5307–5317.
45 S. H. Lin, C. H. Chang, K. K. Liang, R. Chang, Y. J. Shiu, J. M. Zhang, T. S. Yang, M. Hayashi and F. C. Hsu, *Adv. Chem. Phys.*, 2002, **121**, 1–88.
46 D. Beljonne, A. J. Ye, Z. G. Shuai and J. L. Brédas, *Adv. Funct. Mater.*, 2004, **14**, 684–692.
47 S. Di Motta, E. Di Donato, F. Negri, G. Orlandi, D. Fazzi and C. Castiglioni, *J. Am. Chem. Soc.*, 2009, **131**, 6591–6598.
48 L. Wang, Q. Li, Z. Shuai, L. Chen and Q. Shi, *Phys. Chem. Chem. Phys.*, 2010, **12**, 3309–3314.
49 A. Troisi, *Chem. Soc. Rev.*, 2011, **40**, 2347–2358.
50 A. D. Platt, M. J. Kendrick, M. Loth, J. E. Anthony and O. Ostroverkhova, *Phys. Rev. B: Condens. Matter Mater. Phys.*, 2011, **84**, 235209.
51 L. Wang, G. Nan, X. Yang, Q. Peng, Q. Li and Z. Shuai, *Chem. Soc. Rev.*, 2010, **39**, 423–434.
52 E. F. Valeev, V. Coropceanu, D. A. da Silva Filho, S. Salman and J.-L. Brédas, *J. Am. Chem. Soc.*, 2006, **128**, 9882–9886.
53 J. R. Reimers, *J. Chem. Phys.*, 2001, **115**, 9103–9109.
54 O. L. Griffith, N. E. Gruhn, J. E. Anthony, B. Purushothaman and D. L. Lichtenberger, *J. Phys. Chem. C*, 2008, **112**, 20518–20524.
55 T. Sakanoue and H. Sirringhaus, *Nat. Mater.*, 2010, **9**, 736–740.
56 H. Geng, Q. Peng, L. Wang, H. Li, Y. Liao, Z. Ma and Z. Shuai, *Adv. Mater.*, 2012, **24**, 3568–3572.
57 L. J. Wang, Q. Peng, Q. K. Li and Z. Shuai, *J. Chem. Phys.*, 2007, **127**, 044506.
58 Z. Wei, W. Hong, H. Geng, C. Wang, Y. Liu, R. Li, W. Xu, Z. Shuai, W. Hu, Q. Wang and D. Zhu, *Adv. Mater.*, 2010, **22**, 2458–2462.
59 W. Jiang, Y. Zhou, H. Geng, S. Jiang, S. Yan, W. Hu, Z. Wang, Z. Shuai and J. Pei, *J. Am. Chem. Soc.*, 2011, **133**, 1–3.
60 X. D. Tang, Y. Liao, H. Geng and Z.-G. Shuai, *J. Mater. Chem.*, 2012, **22**, 18181–18191.
61 R. S. Sanchez-Carrera, P. Paramonov, G. M. Day, V. Coropceanu and J.-L. Brédas, *J. Am. Chem. Soc.*, 2010, **132**, 14437–14446.
62 H. Geng, Y. Niu, Q. Peng, Z. Shuai, V. Coropceanu and J.-L. Brédas, *J. Chem. Phys.*, 2011, **135**, 104703.
63 V. Coropceanu, M. Malagoli, D. A. da Silva, N. E. Gruhn, T. G. Bill and J. L. Brédas, *Phys. Rev. Lett.*, 2002, **89**, 275503.
64 O. Kwon, V. Coropceanu, N. E. Gruhn, J. C. Durivage, J. G. Laquindanum, H. E. Katz, J. Cornil and J. L. Brédas, *J. Chem. Phys.*, 2004, **120**, 8186–8194.
65 S. Subramanian, S. K. Park, S. R. Parkin, V. Podzorov, T. N. Jackson and J. E. Anthony, *J. Am. Chem. Soc.*, 2008, **130**, 2706.
66 M. L. Tang, A. D. Reichardt, P. Wei and Z. Bao, *J. Am. Chem. Soc.*, 2009, **131**, 5264–5273.
67 S. E. Koh, C. Risko, D. A. da Silva Filho, O. Kwon, A. Facchetti, J.-L. Brédas, T. J. Marks and M. A. Ratner, *Adv. Funct. Mater.*, 2008, **18**, 332–340.
68 Y.-H. Kan, K. Wu, Y.-L. Zhu, L.-M. Hou and Z.-M. Su, *Acta Phys.-Chim. Sin.*, 2010, **26**, 1423–1428.
69 M. J. Frisch, G. W. Trucks and H. B. Schlegel, *et al.*, *GAUSSIAN09, R. A.02*, Gaussian, Inc., Wallingford CT, 2009.
70 Q. Tang, D. Zhang, S. Wang, N. Ke, J. Xu, J. C. Yu and Q. Miao, *Chem. Mater.*, 2009, **21**, 1400–1405.
71 M. Winkler and K. N. Houk, *J. Am. Chem. Soc.*, 2007, **129**, 1805–1815.
72 X.-K. Chen, J.-F. Guo, L.-Y. Zou, A.-M. Ren and J.-X. Fan, *J. Phys. Chem. C*, 2011, **115**, 21416–21428.
73 Z. Liang, Q. Tang, R. Mao, D. Liu, J. Xu and Q. Miao, *Adv. Mater.*, 2011, **23**, 5514.
74 M. Y. Kuo, H. Y. Chen and I. Chao, *Chem.–Eur. J.*, 2007, **13**, 4750.
75 A. Girlando, L. Grisanti, M. Masino, I. Bilotti, A. Brillante, R. G. Della Valle and E. Venuti, *Phys. Rev. B: Condens. Matter Mater. Phys.*, 2010, **82**, 035208.
76 Y. Yi, V. Coropceanu and J.-L. Brédas, *J. Chem. Phys.*, 2012, **137**, 164303.
77 V. Coropceanu, Y. Li, Y. Yi, L. Zhu and J.-L. Brédas, *MRS Bull.*, 2013, **38**, 57–64.
78 H. E. Katz, A. J. Lovinger, J. Johnson, C. Kloc, T. Siegrist, W. Li, Y. Y. Lin and A. Dodabalapur, *Nature*, 2000, **404**, 478.
79 B. A. Jones, M. J. Ahrens, M. H. Yoon, A. Facchetti, T. J. Marks and M. R. Wasielewski, *Angew. Chem., Int. Ed.*, 2004, **43**, 6363–6366.
80 B. A. Jones, A. Facchetti, M. R. Wasielewski and T. J. Marks, *J. Am. Chem. Soc.*, 2007, **129**, 15259.
81 Z. Chen, Y. Zheng, H. Yan and A. Facchetti, *J. Am. Chem. Soc.*, 2009, **131**, 8.
82 H. Yan, Z. Chen, Y. Zheng, C. Newman, J. R. Quinn, F. Dotz, M. Kastler and A. Facchetti, *Nature*, 2009, **457**, 679.
83 J. H. Oh, S. L. Suraru, W. Y. Lee, M. Koenemann, H. W. Hoeffken, C. Roeger, R. Schmidt, Y. Chung, W.-C. Chen, F. Wuerthner and Z. Bao, *Adv. Funct. Mater.*, 2010, **20**, 2148.
84 R. Schmidt, J. H. Oh, Y.-S. Sun, M. Deppisch, A.-M. Krause, K. Radacki, H. Braunschweig, M. Koenemann, P. Erk, Z. Bao and F. Wuerthner, *J. Am. Chem. Soc.*, 2009, **131**, 6215–6228.
85 M. H. Yoon, A. Facchetti, C. E. Stern and T. J. Marks, *J. Am. Chem. Soc.*, 2006, **128**, 5792–5801.

 

86 R. Schmidt, J. Oh, Y. Sun, M. Deppisch, A. Krause, K. Radacki, H. Braunschweig, M. Konemann, P. Erk and Z. Bao, *J. Am. Chem. Soc.*, 2009, **131**, 6215.
87 N. Minder, S. Ono, Z. Chen, A. Facchetti and A. Morpurgo, *Adv. Mater.*, 2012, **24**, 503.
88 A. Molinari, H. Alves, Z. Chen, A. Facchetti and A. Morpurgo, *J. Am. Chem. Soc.*, 2009, **131**, 2462.
89 H. Y. Chen and I. Chao, *ChemPhysChem*, 2006, **7**, 2003–2007.
90 L. Lin, H. Geng, Z. Shuai and Y. Luo, *Org. Electron.*, 2012, **13**, 2763.
91 W. W. Zhang, X. X. Zhong and Y. Zhao, *J. Phys. Chem. A*, 2012, **116**, 11075–11082.
92 Y. Zhao and W. Z. Liang, *Chem. Soc. Rev.*, 2012, **41**, 1075–1087.
93 T. Wakahara, P. D'Angelo, K. i. Miyazawa, Y. Nemoto, O. Ito, N. Tanigaki, D. D. C. Bradley and T. D. Anthopoulos, *J. Am. Chem. Soc.*, 2012, **134**, 7204–7206.
94 S. K. Park, S. Varghese, J. H. Kim, S.-J. Yoon, O. K. Kwon, B.-K. An, J. Gierschner and S. Y. Park, *J. Am. Chem. Soc.*, 2013, **135**, 4757–4764.
95 J. Zhang, J. H. Tan, Z. Y. Ma, W. Xu, G. Y. Zhao, H. Geng, C. A. Di, W. P. Hu, Z. G. Shuai, K. Singh and D. B. Zhu, *J. Am. Chem. Soc.*, 2013, **135**, 558–561.
96 Z. G. Shuai, W. Xu, Q. Peng and H. Geng, *Sci. China: Chem.*, 2013, **56**, 1277–1284.
97 A. Troisi, *J. Chem. Phys.*, 2011, **134**, 034702.
98 A. S. Eggeman, S. Illig, A. Troisi, H. Sirringhaus and P. A. Midgley, *Nat. Mater.*, 2013, **12**, 1045–1049.
99 J. Y. Xi, M. Q. Long, L. Tang, D. Wang and Z. G. Shuai, *Nanoscale*, 2012, **4**, 4348–4369.
100 J. Gao, A. Cembran and Y. R. Mo, *J. Chem. Theory Comput.*, 2010, **6**, 2469–2476.
101 T. Nelson, S. F. Alberti, V. Chernyak, A. E. Roitberg and S. Tretiak, *J. Chem. Phys.*, 2012, **136**, 054108.